Available online at www.sciencedirect.com
SCIENCE DIRECT®
Comput. Methods Appl. Mech. Engrg. 193 (2004) 1277–1303
Computer methods in applied mechanics and engineering
www.elsevier.com/locate/cma

A variational formulation and a double-grid method for meso-scale modeling of stressed grain growth in polycrystalline materials

J.S. Chen [a,*], V. Kotta [a], H. Lu [b], D. Wang [a], D. Moldovan [c], D. Wolf [d]

[a] *Department of Civil and Environmental Engineering, University of California, Los Angeles (UCLA), 5731 Boelter Hall, Los Angeles, CA 90095-1593, USA*
[b] *Department of Mechanical Engineering, Northwestern University, Evanston, IL 60208, USA*
[c] *Department of Mechanical Engineering, Louisiana State University, 2504 CEBA, Baton Rouge, LA 70803, USA*
[d] *Materials Science Division, Argonne National Laboratory, 9700 S. Cass Ave. Argonne, IL 60439, USA*

Received 10 June 2003; received in revised form 6 October 2003; accepted 4 December 2003

Abstract

A deterministic approach for meso-scale modeling of grain growth in stressed polycrystalline materials based on the principle of virtual power is presented. The variational equation is formulated based on the power balance of the system associated with grain boundary surface tension and curvature, rate of strain energy stored in each grain, strain energy density jump across the grain boundaries, and external work rate. The numerical solution of stressed grain growth variational equation requires discretization of grain interiors and grain boundaries. This cannot be effectively modeled by Lagrangian, Eulerian, or Arbitrary Lagrangian Eulerian finite element method if grain boundary migration (moving interfaces) and topological changes of grain boundary geometry are considered. This paper presents a double-grid method to resolve the above mentioned difficulty. In this approach, the material grid points carry material kinematic variables, whereas the grain boundary grid points carry grain boundary kinematic variables. The material domain is discretized by a moving least squares reproducing kernel approximation with strain discontinuity enrichment across the grain boundaries. The grain boundaries, on the other hand, are discretized by the standard finite elements. An interface enrichment function to accurately capture strain jump conditions across the grain boundaries is introduced. A reproducing kernel approximation that includes the periodicity of the unit cell in the construction of reproducing kernel shape function for material velocity is also presented. This proposed double-grid method allows modeling of arbitrary evolution of grain boundaries without remeshing.
© 2004 Elsevier B.V. All rights reserved.

Keywords: Meshfree method; Reproducing kernel approximation; Grain growth; Grain boundary migration; Microstructure evolution

* Corresponding author.
E-mail address: jschen@seas.ucla.edu (J.S. Chen).

0045-7825/$ - see front matter © 2004 Elsevier B.V. All rights reserved.
doi:10.1016/j.cma.2003.12.020

1. Introduction

The microstructure of polycrystalline materials has been observed to have a profound influence on a variety of properties of the material, such as the strength, toughness, electrical conductivity, magnetic susceptibility, etc. For example, it has been shown through experiments that the yield strength of a polycrystalline material increases with a decrease in the grain size [7]. It has been also demonstrated experimentally by Han et al. [15] that the creep rate for power law creep increases with an increase in the grain size. The microstructure is characterized by the grains which evolve due to a complex interplay of a variety of driving forces. The grain growth process occurs by the diffusion and migration of grain boundaries triggered by their tendency to lower the total free energy. Grain boundaries are defined as the interfacial transition regions between two grains differing in their crystallographic orientation.

In the recent years the grain growth processes have been studied by computer simulations. These simulations were broadly classified into statistical and direct simulations [2]. A statistical model does not consider an explicit model for the grain structure but takes into account the distributions of the grain sizes. Statistical models also do not consider the topological constraints [2]. For example, Novikov [29] used this approach to simulate evolution of the grain size distribution and obtained a grain growth exponent of 2.2. Direct simulations, on the other hand, consider an explicit model of the grain structure. They can be further classified into probabilistic and deterministic models.

Probabilistic models are generally of Monte-Carlo type and have their basis in the classical spin models of statistical physics; first identified by Sahni et al. [32]. The most investigated is Potts model [1]. In the Potts model approach grains are subdivided into small-area elements and growth dynamics are simulated by exchange of area elements between grains. Growth takes place as a consequence of the minimization of the internal energy of the system. The exchange step of area elements from one grain to the neighboring grain is carried out using a Monte-Carlo algorithm. The advantage of Monte-Carlo method is its simplicity and the ease of its implementation in two and three-dimensional systems. However, in this method the origin of the stochastic aspect is not clear, nor is the relation between the Monte-Carlo time step and the physical time.

In the deterministic models, the motion of grain boundaries is followed by time integration of their position assuming the normal velocity of the grain boundary to be proportional to the boundary curvature. Deterministic models employ a precise relationship for the velocity for the grain boundaries. A purely deterministic approach was proposed first by Fullman [14] and is referred to as "vertex model". Later, this was improved by Soares et al. [35] and Kawasaki et al. [18] assuming straight grain boundaries. Frost et al. [13] and Weygand and Brechet [44] extended the straight boundary approaches to curved grain boundaries.

The use of Molecular dynamics method for the simulation of grain boundary migration was illustrated by Schönfelder et al. [33]. Molecular dynamics method was used to examine the dependence of the migration rate on the curvature of the grain boundary in [41] and the proportionality of the velocity and the curvature was shown. These simulations were also used to obtain the dependence of mobility on temperature through the Arrhenius relation. Molecular dynamics simulations were also used by Haslam et al. [16,17] and Modolvan et al. [23,24] to demonstrate the effect of the rotations of the grains on the grain evolution process. They reported that the grain growth process is affected by the surface curvature of the grain boundaries and grain rotation induced grain coalescence.

The use of variational approach for modeling the grain growth had started gaining attention due to the flexibility of the approach which can easily incorporate different physical processes affecting grain growth. It was first proposed by Needleman and Rice [28] for dissipative systems and was later used by Cocks and Gill [8] for the curvature-driven grain growth process. Their modification describes the rate of power dissipation due to the competition between the reduction in the grain boundary energy and the viscous drag during grain boundary migration. Moreover, the grain boundaries were discretized using finite elements. Sun and Suo [36] further extended the approach to include the diffusion effect. Variational principle has been used in modeling grain boundary diffusion by Pan and Cocks [31] for arbitrary grain structure and was

later coupled with surface diffusion by Pan and Cocks [30] where they proposed a numerical scheme to solve the coupled diffusion problem. The flexibility of the variational method has also been utilized to study a variety of different phenomena such as void growth [28], dislocation climb [37], and solid state sintering [10,22,38].

When a polycrystalline microstructure is subjected to an externally applied stress, an additional driving force, in addition to that resulting from the grain boundary curvature, has to be considered. This is due to the elastic anisotropy of the grains comprising the microstructure, which in general store different amounts of elastic energy densities. Our focus in this study is to investigate the grain growth in the presence of both curvature driven and stress induced grain boundary migration. In this work, we introduce a variational equation based on the balance of powers associated with grain boundary surface tension and curvature, elastic strain energy rate, and the elastic strain energy density difference due to anisotropy between adjacent grains. This reflects the coupling of elastic deformation of grains with grain boundary migration and thus necessitates the discretization of grain boundaries and grain domains. Using finite element method to study the migration of grain boundaries leads to a severe mesh distortion in each grain, and the topological changes of grain structures further demand a complete remeshing. To address the above mentioned issues, a double-grid method is proposed. The elastic deformation of grains is modeled by a reproducing kernel discretization with built-in strain discontinuities along the grain boundaries [6,43], whereas the migration velocity on grain boundaries is modeled using the standard finite element approximation.

The layout of this paper is as follows. Grain growth kinematics and the geometry of polycrystalline system are briefly reviewed in Section 2. In Section 3, the variational formulation for boundary migration under stress is presented. The doubled-grid discretization and formulation for grain boundary and material domains are introduced in Section 4. Methods for incorporating strain discontinuity across grain boundaries as well as for enhancing solution due to periodicity are also discussed in this section. Section 5 demonstrates that the evolution of grain growth can be effectively simulated without any remeshing through numerical examples. Concluding remarks are given in Section 6.

2. Grain growth kinematics and polycrystalline geometry

Grain boundary migration is the motion of the interface between two crystals or grains caused by a wide variety of driving forces. Grain Boundary migration is the primary cause of the growth of the grains in polycrystalline materials. Grain boundary migration does not involve the nucleation of new grains but it involves the growth of already existing grains at the expense of the other preexisting grains in the grain network [39]. As a result the average size of the grains increase which is accompanied by a reduction in the total grain boundary energy per unit volume.

2.1. Grain boundaries migration driving forces

Migration of grain boundaries occurs due to a wide variety of driving forces. The origin is the tendency of the grain boundaries to reduce its total surface free energy, which is accomplished by the reduction of the total grain boundary area. Let f_n be the driving force which contributes to the reduction of the total free energy of the grain network accomplished by the grain interface motion. The kinetic law which relates this force to the normal velocity of the grain boundary following [27,26,40] is

$$v_n = \mu f_n, \tag{2.1}$$

where μ is the mobility which represents the ease with which the grain boundary can migrate and is dependent on the temperature through the relation [4]

$$\mu = M_0 \mathrm{e}^{-Q/KT}, \tag{2.2}$$

where Q is the activation enthalpy associated with the motion, K is the Boltzmann constant, and M_0 has a weak dependence on temperature.

The most important driving force triggering grain boundary migration is the force due to the curvature of the interface (grain boundary) which is called the capillarity force:

$$f_c = \gamma(\theta)\left(\frac{1}{R_1} + \frac{1}{R_2}\right), \tag{2.3}$$

where γ is the surface tension (the boundary energy per unit area) which is a function of the misorientation of the grain boundary θ, and R_1, R_2 are the principal radii of curvature of the surface. This force acts towards its center of curvature, and it reduces the boundary energy through the reduction in grain boundary area.

In general at small grain sizes the most significant driving force for grain boundary migration is the surface tension. However, at larger grain sizes and in the presence of strain energy, additional driving forces [9] due to the difference in elastic strain energy densities in the volumes of neighboring grains, may also play a key role in grain boundary migration. For instance, this driving force f_e can be expressed as:

$$f_e = \frac{|\Delta U|}{\Delta V}, \tag{2.4}$$

where ΔU is the difference in the strain energy stored in volume ΔV between adjacent grains, and ΔV is the volume through which the grain boundary segment has swept during a migration step.

2.2. Topology of polycrystalline geometry

The phenomenon of grain growth accompanies the increase in size of some preexisting grains at the expense of other preexisting grains. This involves the disappearance of some of the grains which leads to a topological reconstruction of the entire grain structure. For computer simulation of grain growth, it is necessary to clearly define rules governing the topological reconstruction of the grain network. These rules are discussed in this section. Smith [34] described the topological requirements of a grain network. Let N, V, and E be the numbers of grains, vertices, and grain boundaries, respectively as shown in Fig. 1, the grain structure in two-dimensional space obeys the Euler's equation:

$$N + V - E = 1. \tag{2.5}$$

In 2D, a grain network with more than three grain boundaries intersecting at a point is topologically unstable. Thus a topologically stable grain network will have only three grain boundaries intersecting at a vertex which is called the triple point. The following geometric relation exists in grain network [12]:

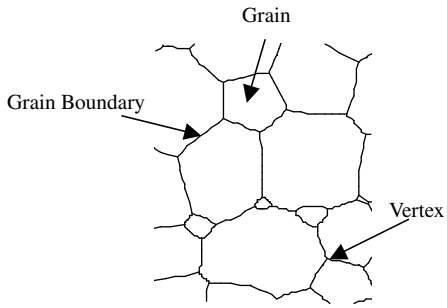

Fig. 1. 2D grain structure.

$$3V = 2E = \bar{n}N, \tag{2.6}$$

where $\bar{n}$ is the mean number of vertices per grain. For a system with a large number of grains ($N \gg 1$), $\bar{n} = 6$.

Morral and Ashby [25] identified two types of grain topology transformations, namely the disappearance or appearance of a three sided grain and the interchange of grain neighbors. These changes were denoted as the T1 and T2 changes. A T1 change involves the switching of the grain boundaries when two triple points come very close to each other. This leads to topological instability in the grain network and results in the formation of a new grain boundary. The result is that two grains lose an edge while two other grains gain an edge, thus maintaining the total number of edges and grains in the grain network as shown in Fig. 2. This transformation is called the topological change of the first kind. In Numerical simulations, the 'T1' change is done by rotating the grain boundary to be switched by 90° as shown in the Fig. 2 with the length of the grain boundary slightly increased such that the boundary does not undergo a T1 change immediately.

T2 represents the topological change of second kind where a three sided grain shrinks to a point as shown in Fig. 3. After this topological transformation, all the neighbors of the three sided grain lose a side each and the total number of grains and edges are decreased. In simulations, this three sided grain is replaced by a triple point at the centroid of the grain and the grain boundary connectivity is updated accordingly.

In numerical simulations, a 'T1' change might result in a two sided grain which again leads to topological instability in the grain network. This two sided grain is replaced by a single grain boundary and this topological transformation is called the third kind or a 'T3' change as shown in Fig. 4.

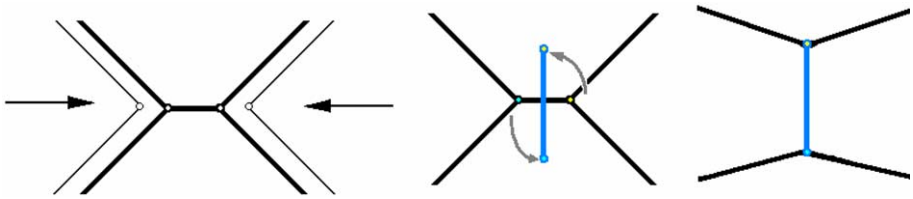

Fig. 2. Topological change of the first kind (T1).

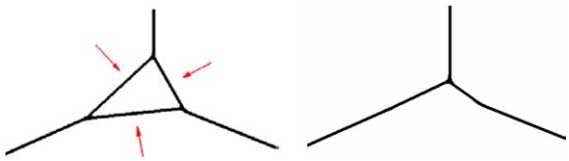

Fig. 3. Topological change of the second kind (T2).

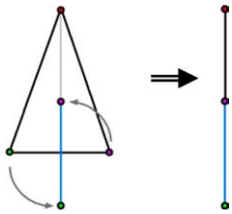

Fig. 4. Topological change of the third kind (T3).

3. Variational formulation of stressed grain growth

Consider a two-dimensional domain Ω consisting of grains with grain boundary network Γ_{gb} and external boundary Γ, and the unit cell microstructure is subjected to an external traction as shown in Fig. 5. In this section, virtual powers due to the system associated with grain boundary surface tension and curvature, energy dissipation, rate of strain energy stored in each grain, strain energy density jump across the grain boundaries, and external work rate will be discussed, and finally the variational equation based on the principle of virtual power will be obtained.

3.1. Rate of virtual work done by virtual grain boundary tension

We start with a virtual grain boundary migration with a virtual velocity $\delta\bar{v}_n$ normal to the grain boundary and a virtual velocity $\delta\bar{v}_s$ along the arc length of the boundary as shown in Fig. 6. Using the property

$$\mathrm{d}\bar{v}_s = \left(\bar{v}_s + \frac{\partial \bar{v}_s}{\partial s}\,\mathrm{d}s\right)\cos\mathrm{d}\theta - \bar{v}_s + \left(\bar{v}_n + \frac{\partial \bar{v}_n}{\partial s}\,\mathrm{d}s\right)\sin\mathrm{d}\theta \tag{3.1}$$

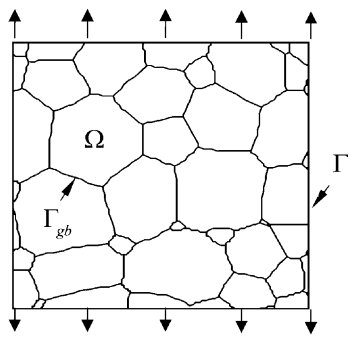

Fig. 5. Unit cell microstructure of stressed grain network.

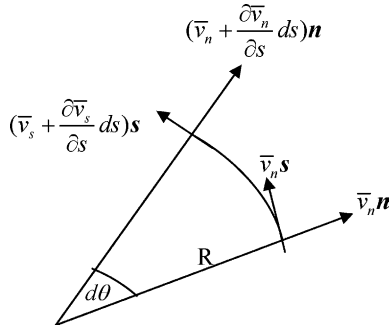

Fig. 6. Segment of a grain boundary.

or,

$$\mathrm{d}\bar{v}_s = \frac{\partial \bar{v}_s}{\partial s}\,\mathrm{d}s\cos\mathrm{d}\theta + \left(\bar{v}_n + \frac{\partial \bar{v}_n}{\partial s}\,\mathrm{d}s\right)\sin\mathrm{d}\theta \tag{3.2}$$

and further considering for very small angle $\mathrm{d}\theta$, $\sin\mathrm{d}\theta \approx \mathrm{d}\theta$, $\cos\mathrm{d}\theta \approx 1$, and thus

$$\mathrm{d}\bar{v}_s = \frac{\partial \bar{v}_s}{\partial s}\,\mathrm{d}s + \bar{v}_n\mathrm{d}\theta. \tag{3.3}$$

The virtual rate of elongation of the grain boundary per unit length is obtained as

$$\mathrm{d}\bar{v}_s = \frac{\partial \bar{v}_s}{\partial s}\,\mathrm{d}s + \bar{v}_n\mathrm{d}\theta. \tag{3.4}$$

Note that the local grain boundary curvature is

$$k = \frac{1}{R} = \frac{\mathrm{d}\theta}{\mathrm{d}s}, \tag{3.5}$$

where R is the radius of curvature of the grain boundary, thus

$$\delta\dot{\varepsilon}_s = \frac{\partial \delta\bar{v}_s}{\partial s} + \delta\bar{v}_n k. \tag{3.6}$$

Thus the rate of virtual work done by the surface tension is

$$\delta\dot{W}_1 = \int_{\Gamma_{\mathrm{gb}}} \gamma\delta\dot{\varepsilon}_s\,\mathrm{d}s = \int_{\Gamma_{\mathrm{gb}}} \gamma\left(\frac{\partial \delta\bar{v}_s}{\partial s} + \frac{\delta\bar{v}_n}{R}\right)\mathrm{d}s, \tag{3.7}$$

where γ is the surface tension which has a dominant effect at small length scales and the integration is carried on all the grain boundaries.

3.2. Rate of virtual energy dissipation on grain boundaries

The rate of virtual energy dissipation resulting from the viscous drag due to the virtual grain boundary motion is

$$\delta\dot{W}_2 = \int_{\Gamma_{\mathrm{gb}}} f_n\delta\bar{v}_n\,\mathrm{d}s, \tag{3.8}$$

where the driving force f_n is related to the velocity $\bar{v}_n$ through the kinetic law [26,27,40]

$$\bar{v}_n = \mu f_n. \tag{3.9}$$

Here, μ is the mobility of the grain boundary motion which. Thus Eq. (3.9) becomes

$$\delta\dot{W}_2 = \int_{\Gamma_{\mathrm{gb}}} \frac{1}{\mu}\bar{v}_n\delta\bar{v}_n\,\mathrm{d}s. \tag{3.10}$$

3.3. Strain energy density effect

In a system in which there is a variation in the material elastic properties of any two adjacent grains, the strain energy density in the two regions on the opposite side of a grain boundary is in general different. Therefore, when an external stress is considered, besides the capillarity force, there is an additional contribution to the driving force acting on a grain boundary due to the difference in the strain energy density

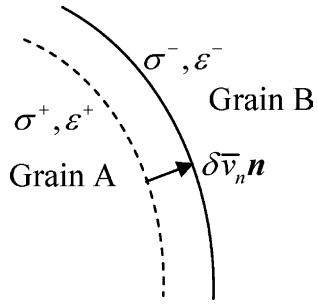

Fig. 7. Strain energy density change due to grain boundary migration.

rate across the grain boundary. The virtual power corresponding to the virtual velocity of the grain boundary $\delta\bar{v}_n$ can be written as

$$\delta\dot{W}_3 = \int_{\Gamma_{\mathrm{gb}}} \frac{1}{2}(\boldsymbol{\sigma}^+ : \boldsymbol{\varepsilon}^+ - \boldsymbol{\sigma}^- : \boldsymbol{\varepsilon}^-)\delta\bar{v}_n \,\mathrm{d}\Gamma, \tag{3.11}$$

where $\boldsymbol{\sigma}^+$, $\boldsymbol{\varepsilon}^+$ are the stress and strain in the grain that gains virtual area $\delta\bar{v}_n \,\mathrm{d}\Gamma$ per unit time (Fig. 7, grain A), respectively, and $\boldsymbol{\sigma}^-$, $\boldsymbol{\varepsilon}^-$ are the stress and strain in the grain located on the other side of the boundary (Fig. 7, grain B), respectively. An anisotropic creep law is considered for each grain

$$\sigma_{ij} = C_{ijkl}\dot{\varepsilon}_{kl}, \tag{3.12}$$

where $\dot{\varepsilon}_{ij}$ is the strain rate given by

$$\dot{\varepsilon}_{ij} = \frac{1}{2}\left(\frac{\partial v_i}{\partial x_j} + \frac{\partial v_j}{\partial x_i}\right) \tag{3.13}$$

and v_i is the material velocity.

By adding virtual power terms of Eqs. (3.7), (3.10) and (3.11), with further consideration of the virtual power associated with the strain energy stored in all grains and the external virtual work rate done by surface traction and body force, the following variational equation is obtained

$$\int_\Omega \delta\dot{\boldsymbol{\varepsilon}} : \boldsymbol{\sigma}\,\mathrm{d}\Omega + \left(\int_{\Gamma_{\mathrm{gb}}} \gamma\left(\frac{\partial\delta\bar{v}_s}{\partial s} + \frac{\delta\bar{v}_n}{R}\right)\mathrm{d}s + \int_{\Gamma_{\mathrm{gb}}} \frac{\delta\bar{v}_n}{\mu}\bar{v}_n\,\mathrm{d}s\right) + \frac{1}{2}\int_{\Gamma_{\mathrm{gb}}} \delta\bar{v}_n(\boldsymbol{\sigma}^+ : \boldsymbol{\varepsilon}^+ - \boldsymbol{\sigma}^- : \boldsymbol{\varepsilon}^-)\,\mathrm{d}\Gamma$$
$$- \int_{\Gamma_h} \delta\boldsymbol{v}\cdot\boldsymbol{h}\,\mathrm{d}\Gamma - \int_\Omega \delta\boldsymbol{v}\cdot\boldsymbol{b}\,\mathrm{d}\Omega = 0. \tag{3.14}$$

It is noted that the periodic boundary conditions are imposed on the boundaries of unit cell for $\boldsymbol{v}$ and $\bar{\boldsymbol{v}}$:

$$(\boldsymbol{v} - \boldsymbol{v}_0)|_{\Gamma^+} = (\boldsymbol{v} - \boldsymbol{v}_0)|_{\Gamma^-}, \tag{3.15}$$

$$\bar{\boldsymbol{v}}|_{\Gamma^+} = \bar{\boldsymbol{v}}|_{\Gamma^-}, \tag{3.16}$$

where Γ^+ and Γ^- represent the opposite boundaries, and $\boldsymbol{v}_0$ represents the material velocity of the reference point on the boundary.

4. Discretization of grain evolution equations by a double-grid method

Eq. (3.14) can be viewed as the stationary condition of the Gibb's free energy associated with the stressed grain network. The grain structures will migrate and deform in response to the grain boundary

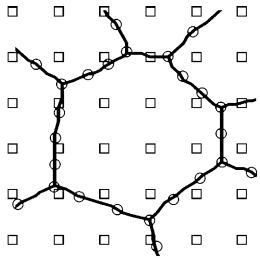

□ Material point ○ Grain boundary point

Fig. 8. Double-grid discretization.

driving forces as well as the external work so as to minimize the total Gibb's free energy. Through the grain boundary migration progresses, the grain structures will undergo topological changes as described in Section 2. Thus finite element discretization of grain material velocity $\boldsymbol{v}$ in each grain domain and grain boundary velocity $\bar{\boldsymbol{v}}$ will require a continuous remeshing which is tedious and time consuming. In this work, a double-grid method is proposed as shown in Fig. 8. The material domain is discretized by uniformly distributed material points carrying material velocity $\boldsymbol{v}$, whereas the grain boundary is discretized by the grain boundary points carrying grain boundary velocity $\bar{\boldsymbol{v}}$. The material velocity is approximated by a moving least square reproducing kernel approximation with strain discontinuity along material interface [43]. The grain boundary velocity is approximated by the standard finite element shape function along the grain boundaries. This section discusses the approximation of $\boldsymbol{v}$ and $\bar{\boldsymbol{v}}$ using this double-grid approach and the resulting discrete equations for grain deformation and grain boundary migration.

4.1. Double-grid approximation

For simplicity, the grain boundary velocity $\bar{\boldsymbol{v}}$ is approximated by the standard finite element shape function. The approximation of material velocity $\boldsymbol{v}$, on the other hand, requires the following properties: (1) smooth (at least C^0) inside the grain domain, and (2) discontinuous in its derivative normal to the evolving grain boundary. Several approaches to deal with interface conditions have been introduced [11,19,43]. In this work, we introduce the following approximation for $\boldsymbol{v}$ and $\bar{\boldsymbol{v}}$:

$$v_i(\boldsymbol{x}) = \sum_{I=1}^{\mathrm{NP}} \Psi_I(\boldsymbol{x}) \upsilon_{iI} + \sum_{I=1}^{\mathrm{NS}} \widehat{\Psi}_I(\boldsymbol{x}) \beta_{iI}, \tag{4.1}$$

$$\bar{v}_i(s) = \sum_{I=1}^{\mathrm{NS}} N_I(s) \bar{\upsilon}_{iI}, \tag{4.2}$$

where Ψ_I's are a set of reproducing kernel shape functions defined at the material points, $\widehat{\Psi}_I$'s are the interface enrichment functions defined at the interface points, $N_I(s)$'s are a set of finite element shape functions defined at the grain boundary points, υ_{iI}, β_{iI}, and $\bar{\upsilon}_{iI}$ are coefficients of the approximation, 'NP' is the number of material points, and 'NS' is the number of grain boundary points.

Remark. Although C^0 continuity is sufficient for Ψ_I, higher order continuity in Ψ_I avoids artificial driving force resulting from inappropriate jumps of strain energy density.

The function Ψ_I is a smooth function formulated based on moving least squares [3,19] and reproducing kernel approximation [20,21]:

$$\Psi_I(\mathbf{x}) = \left[\sum_{i+j=0}^{n} (x_1 - x_{1I})^i (x_2 - x_{2I})^j b_{ij}(\boldsymbol{x})\right] \Phi_a(\boldsymbol{x} - \boldsymbol{x}_I), \tag{4.3}$$

where $\Phi_a(\boldsymbol{x} - \boldsymbol{x}_I)$ is a kernel function, and $b_{ij}(\boldsymbol{x})$ are the coefficients to be solved. The enrichment $\widehat{\Psi}_I$ is constructed as [19]:

$$\widehat{\Psi}_I(\boldsymbol{x}) = \varphi(r)\phi_I(s), \tag{4.4}$$

where and r and s are normal to and along Γ_{gb}, respectively, as shown in Fig. 9. The function $\varphi'(r) \in C^{-1}$ contains derivative discontinuities on Γ_{gb}, and $\phi_I(s)$ is a smooth kernel function along Γ_{gb} as demonstrated in Fig. 10 where the resulting interface enrichment function $\widehat{\Psi}_I$ and $\frac{\partial \widehat{\Psi}_I}{\partial r}$ are also shown. At the triple junction, the enrichment function $\phi(r)$ is constructed as

$$\phi(\boldsymbol{r}) = \phi(r_1) + \phi(r_2) + \phi(r_3) + \phi(r_1)\phi(r_2) + \phi(r_2)\phi(r_3) + \phi(r_1)\phi(r_3) + \phi(r_1)\phi(r_2)\phi(r_3), \tag{4.5}$$

where r_1, r_2, r_3 are the local coordinates of the three grain boundaries that form the triple junction. The corresponding interface functions and their derivatives are shown in Fig. 11.

Coefficient vector $b_{ij}(\boldsymbol{x})$ in Eq. (4.3) is obtained by imposing nth order reproducing conditions:

$$\sum_I \Psi_I(\boldsymbol{x}) x_{1I}^i x_{2I}^j + \sum_I \widehat{\Psi}_I(\boldsymbol{x}) x_{1I}^i x_{2I}^j = x_1^i x_2^j \quad \text{for } 0 \leqslant i + j \leqslant n, \tag{4.6}$$

where the summation in each term is only performed on the nodes where the approximation functions are non-zero at the evaluation location $\boldsymbol{x}$. By substituting Eq. (4.3) into Eq. (4.6), one obtains

$$\boldsymbol{b}(\boldsymbol{x}) = [b_{00}(\boldsymbol{x}), b_{10}(\boldsymbol{x}), b_{01}(\boldsymbol{x})]^{\mathrm{T}} = \boldsymbol{M}^{-1}(\boldsymbol{x})[\boldsymbol{H}(\boldsymbol{0}) - \widehat{\boldsymbol{F}}(\boldsymbol{x})], \tag{4.7}$$

where

$$\boldsymbol{H}^{\mathrm{T}}(\boldsymbol{x} - \boldsymbol{x}_I) = [1, x_1 - x_{1I}, x_2 - x_{2I}], \tag{4.8}$$

$$\boldsymbol{M}(\boldsymbol{x}) = \sum_{I=1}^{\mathrm{NP}} \boldsymbol{H}(\boldsymbol{x} - \boldsymbol{x}_I)\boldsymbol{H}^{\mathrm{T}}(\boldsymbol{x} - \boldsymbol{x}_I)\Phi_a(\boldsymbol{x} - \boldsymbol{x}_I), \tag{4.9}$$

$$\widehat{\boldsymbol{F}}(\mathbf{x}) = \sum_{I=1}^{\mathrm{NS}} \widehat{\Psi}_I(\boldsymbol{x})\boldsymbol{H}(\boldsymbol{x} - \boldsymbol{x}_I). \tag{4.10}$$

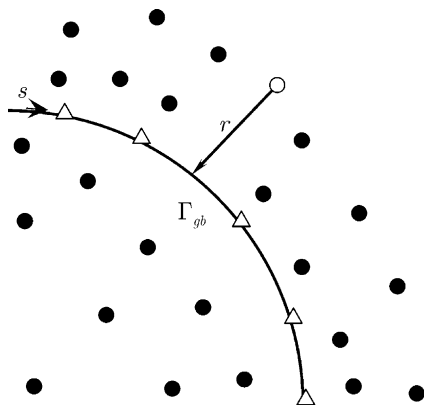

Fig. 9. Discretization of material interface.

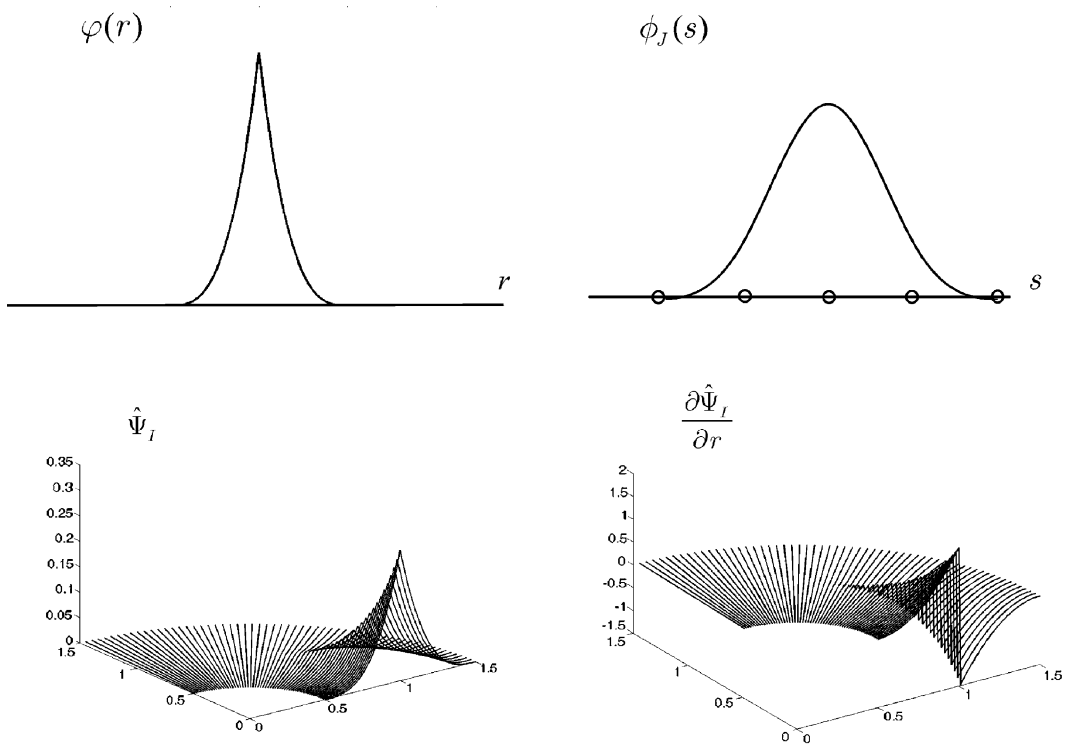

Fig. 10. Interface enrichment function and its derivative.

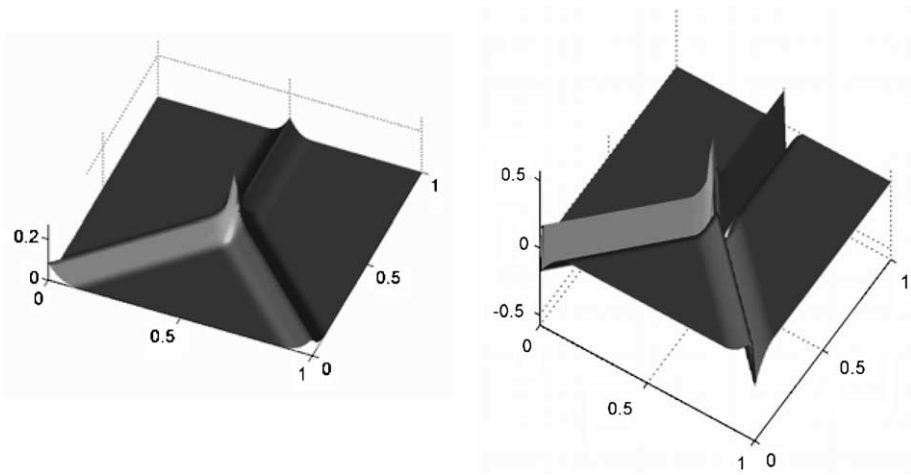

Fig. 11. Interface function and its derivative at the triple junction.

Finally the reproducing kernel shape function takes the form

$$\Psi_I(\boldsymbol{x}) = \boldsymbol{H}^{\mathrm{T}}(\boldsymbol{x} - \boldsymbol{x}_I)\boldsymbol{M}^{-1}(\boldsymbol{x})[\boldsymbol{H}(\boldsymbol{0}) - \widehat{\boldsymbol{F}}(\boldsymbol{x})]\Phi_a(\boldsymbol{x} - \boldsymbol{x}_I). \tag{4.11}$$

Since $\widehat{\Psi}_I(\boldsymbol{x})$ is introduced locally on the material interface, for point $\boldsymbol{x}$ that is not covered by the influence zone of the interface enrichment functions, $\widehat{\Psi}_I(\boldsymbol{x})$ vanishes, and Eq. (4.11) reduces to the standard reproducing kernel shape function.

In summary, the interface-enriched reproducing kernel approximation of Eq. (4.11) can be written in the following form:

$$v_i(\boldsymbol{x}) = \sum_{I=1}^{\mathrm{NP+NS}} \Psi_I(\boldsymbol{x}) v_{iI}, \tag{4.12}$$

$$\Psi_I(\boldsymbol{x}) = \begin{cases} \widehat{\Psi}_I(\boldsymbol{x}) & \text{for } I : \boldsymbol{x}_I \in \Gamma_{\mathrm{gb}}, \\ \boldsymbol{H}^{\mathrm{T}}(\boldsymbol{x} - \boldsymbol{x}_I)\boldsymbol{M}^{-1}(\boldsymbol{x})[\boldsymbol{H}(\boldsymbol{0}) - \widehat{\boldsymbol{F}}(\boldsymbol{x})]\Phi_a(\boldsymbol{x} - \boldsymbol{x}_I) & \text{otherwise.} \end{cases} \tag{4.13}$$

The coupling between the reproducing kernel shape function and interface enrichment shape function according to Eq. (4.13) is shown in Fig. 12.

Two test problems are analyzed below using the proposed approach for interface conditions.

A one-dimensional bi-material bar as shown in Fig. 13 is subjected to a body force $b(x) = a_0 + a_1 x + a_2 x^2 + a_3 x^3$ with $a_0 = 0$, $a_1 = 25$, $a_2 = -7.5$, $a_3 = 0.5$. The elastic moduli of the two materials are $E_1 = 10,000$ and $E_2 = 1000$. Two methods are compared: (1) RKPM: solving elasticity problem with reproducing kernel particle method without interface enrichment function, (2) I-RKPM: solving elasticity problem with reproducing kernel particle method (RKPM) [20,21] and interface enrichment function. Total of 11 points are used to discrete problem domain for both cases. Due to a smooth kernel in RKPM, the strain is highly oscillatory as shown in Fig. 14 for case (1). This deficiency can be corrected by I-RKPM without increasing the degrees of freedom.

The next test problem is a circular inclusion with a constant eigen-strain ε^0 embedded in an infinite matrix as shown in Fig. 15. The exact solution of displacement for this problem is

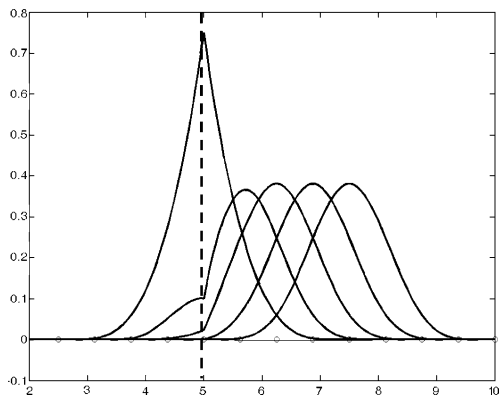

Fig. 12. Coupling between interface enrichment function and the reproducing kernel function.

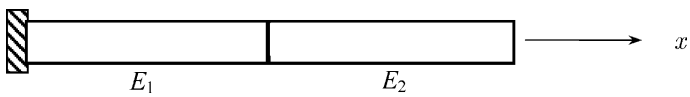

Fig. 13. One-dimensional bi-material rod.

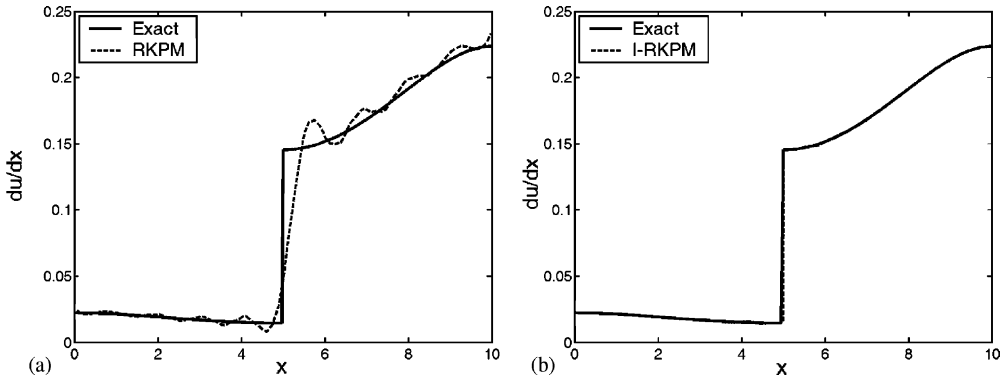

Fig. 14. Strain distribution of 1D rod with body force: (a) RKPM and (b) I-RKPM.

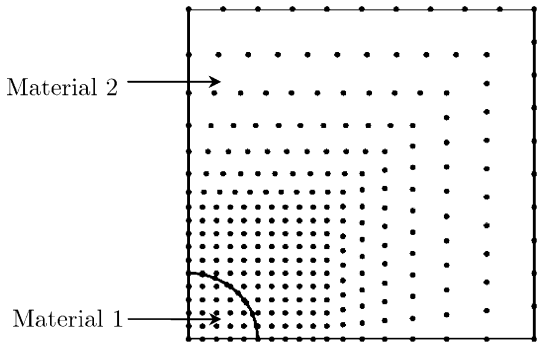

Fig. 15. Discretization of a 2D bi-material plate.

$$u_r = \begin{cases} C_1 r & r \leqslant R, \\ C_1 \dfrac{R^2}{r} & r \geqslant R \end{cases} \tag{4.14}$$

and the corresponding radial strain field is

$$\varepsilon_{rr} = \begin{cases} C_1, & r \leqslant R, \\ -C_1 \dfrac{R^2}{r^2}, & r \geqslant R, \end{cases} \tag{4.15}$$

$$C_1 = \frac{(\lambda_1 + \mu_1)\varepsilon^0}{\lambda_1 + \mu_1 + \mu_2}, \tag{4.16}$$

where R is the radius of inclusion, λ_i and μ_i are Lame constants of material phases: $i = 1$ for inclusion and $i = 2$ for matrix, and ε^0 denotes the prescribed constant volumetric eigen-strain in the inclusion.

The material constants used for this example are $\lambda_1 = 497.16$, $\mu_1 = 390.63$, $\lambda_2 = 656.79$, and $\mu_1 = 338.35$. The volumetric eigen-strain ε^0 in the inclusion has a value of 0.01. Due to twofold symmetry, only one quarter of the domain is used as shown in Fig. 15, where each side of the domain has length 5, and the radius R of the inclusion is unity. Exact displacement boundary conditions are imposed on the top and right surfaces, and symmetric conditions are imposed on the bottom and left surfaces. The radial strains using RKPM and I-RKPM are compared in Fig. 16, where it can be seen that I-RKPM resulted in much higher accuracy.

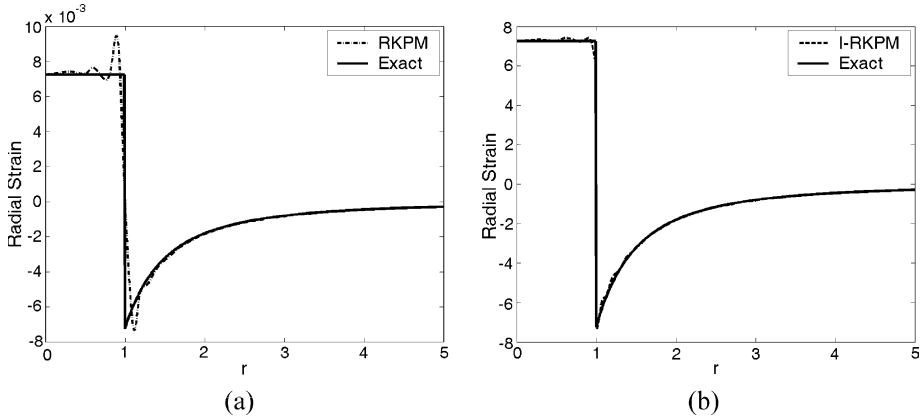

Fig. 16. Comparison of radial strains: (a) RKPM and (b) I-RKPM.

4.2. Treatment of periodicity in MLS/RK approximation

The unit cell of stressed grain growth requires imposition of periodic boundary conditions. MSL/RK shape functions are typically nonlocal and the support of each shape function covers several neighbor particles. This leads to errors in imposing periodic boundary conditions as the shape functions intersect one boundary do not "rape over" to the opposite boundary to represent periodicity. As shown in Fig. 17, the shape functions are truncated near the boundaries, and a fully periodic discrete operator cannot be constructed in one periodic domain.

Periodicity implies infinite repeated domains with periodic conditions over period λ, i.e.,:

$$u(x) = u(x + n\lambda), \quad n = \pm 1, \pm 2, \pm 3, \ldots \tag{4.17}$$

To achieve periodicity in meshfree discretization, additional exterior dump nodes are considered in the approximation of unknowns as shown in Fig. 18. For particle distribution of Fig. 18, the enhanced approximation is expressed as

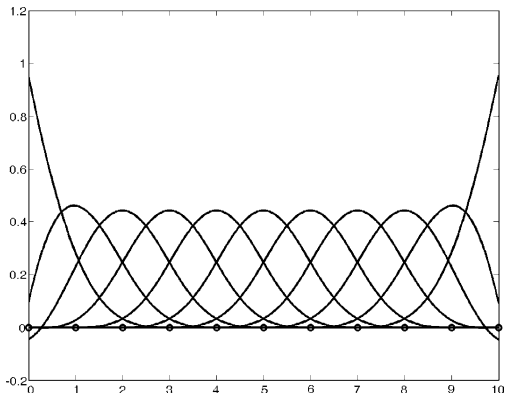

Fig. 17. One-dimensional meshfree shape function in a unit cell.

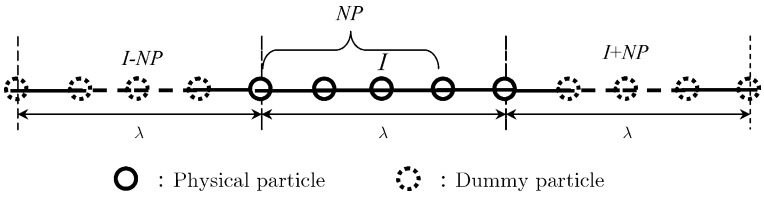

Fig. 18. A 1D periodic domain with dummy particles.

$$u^h(x) = \sum_{I=-m}^{\mathrm{NP}+m} \Psi_I(x) d_I, \quad \forall x \in \Omega, \tag{4.18}$$

where Ω is the physical domain of the unit cell discretized by 'NP' particle. In Eq. (4.18), the summation sums over all physical and dummy particles where their associated shape function supports cover x. By imposing periodicity $d_I = d_{I-\mathrm{NP}} = d_{I+\mathrm{NP}}$ and using static condensation, we obtain the following condensed approximation by 'NP' physical nodes:

$$u^h(x) = \sum_{I=0}^{\mathrm{NP}} \overline{\Psi}_I(x) d_I, \quad \forall x \in \Omega, \tag{4.19}$$

where

$$\overline{\Psi}_I(x) = \Psi_I(x) + \Psi_{I+\mathrm{NP}}(x) + \Psi_{I-\mathrm{NP}}(x). \tag{4.20}$$

Similar approach is applicable to two-dimension. Fig. 19 shows a repeated structure of a 2D unit cell with physical and dummy particles. By periodicity and static condensation, the approximation can be constructed by physical particles with the following corrected shape functions

$$\overline{\Psi}_I(\boldsymbol{x}) = \sum_{J \in G_I} \Psi_J(\boldsymbol{x}), \tag{4.21}$$

where $G_I = \{I, I_1', I_1'', I_2', I_2''\}$ denotes a group of periodic particles associated with node I, which includes the particles with repeated period from node I as shown in Fig. 19.

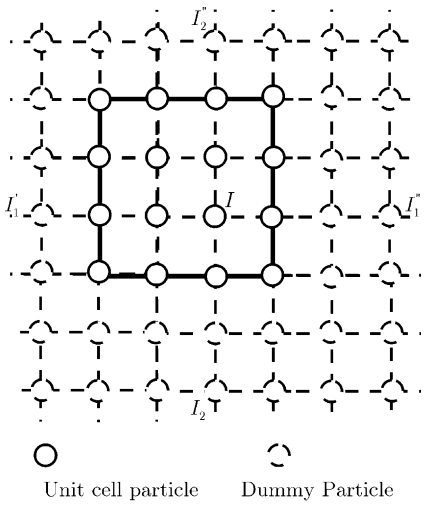

Fig. 19. A repeated structure of 2D unit cell.

To illustrate the effectiveness of the proposed enhanced approximation in dealing with periodicity, consider the following one-dimensional periodic problem

$$\begin{aligned} &u_{,xx} + \sin(2x) = 0 \quad \text{in } (0, 2\pi), \\ &u(0) = u(2\pi) = 0. \end{aligned} \tag{4.22}$$

The corresponding periodic exact solution is

$$u(x) = \tfrac{1}{4}\sin(2x). \tag{4.23}$$

Meshfree solution with 7-node discretization using standard RKPM with MLS/RK approximation and the enhanced approach are compared in Fig. 20(a) and (b). Clearly, much improved solution accuracy is achieved with the proposed approach.

Next, consider now a 2D example with the following governing equation

$$\begin{aligned} &\nabla^2 u + 20\pi^2 \sin(4\pi x)\sin(2\pi y) = 0 \quad \text{in } \Omega = (0,1) \oplus (0,1), \\ &u(0,y) = u(1,y) = u(x,0) = u(x,1) = 0. \end{aligned} \tag{4.24}$$

The corresponding periodic exact solution is

$$u(x,y) = \sin(4\pi x)\sin(2\pi y). \tag{4.25}$$

The analytical solution of $u_{,x}$ is plotted in Fig. 21. A 7×7 uniform discretization is used to model the problem domain Ω. The errors of $u_{,x}$ obtained by both conventional and enhanced RKPM are plotted in Fig. 22(a) and (b), respectively, and the accuracy of the enhanced RKPM solution is clearly better.

4.3. Finite element discretization on grain boundaries

On each segment of grain boundary, the material velocity $\bar{\boldsymbol{v}}$ is approximated by 1-dimensional finite element shape functions

$$\bar{\boldsymbol{v}}^h = \begin{bmatrix} \bar{v}_1^h \\ \bar{v}_2^h \end{bmatrix} = \begin{bmatrix} \sum_I N_I \bar{v}_{I1} \\ \sum_I N_I \bar{v}_{I2} \end{bmatrix} = \sum_I \boldsymbol{N}_I \bar{\boldsymbol{v}}_{\boldsymbol{I}}, \tag{4.26}$$

where

$$\boldsymbol{N}_I = \begin{bmatrix} N_I & 0 \\ 0 & N_I \end{bmatrix}, \tag{4.27}$$

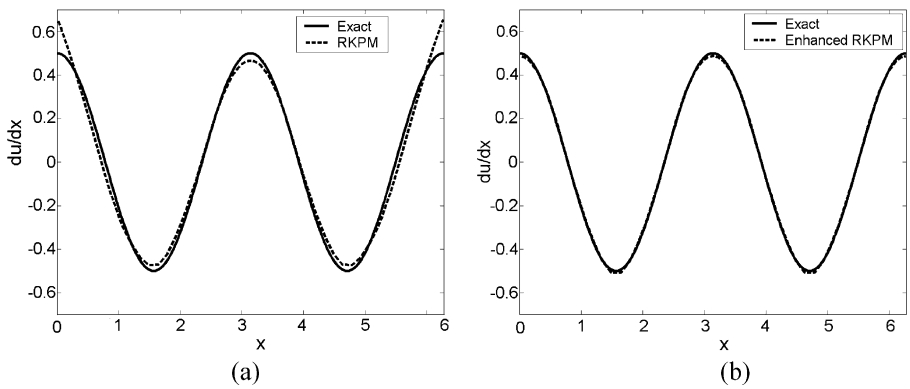

Fig. 20. Solution of Eq. (4.22) using (a) standard RKPM, ND (b) enhanced RKPM.

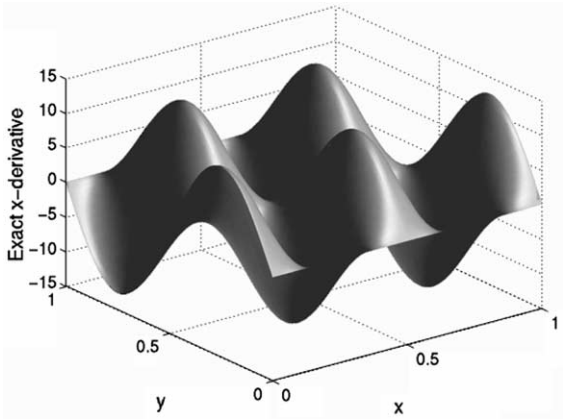

Fig. 21. Analytical solution of $u_{,x}$ for problem (4.24).

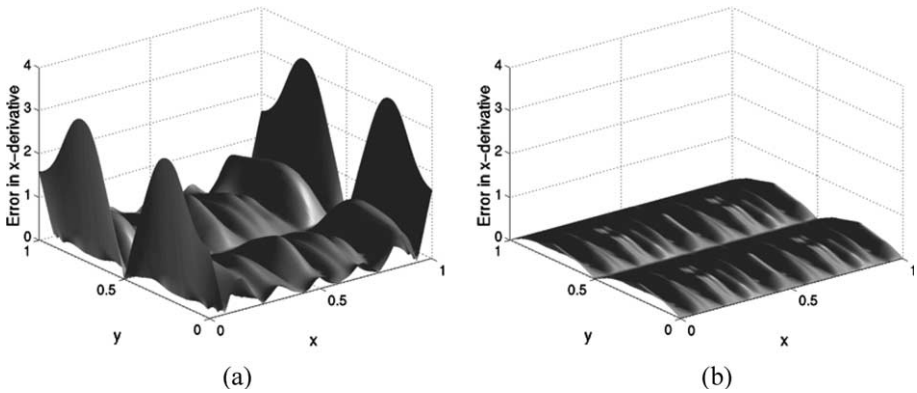

Fig. 22. Errors of $u^h_{,x}$ of (4.24) using (a) standard RKPM, and (b) enhanced RKPM.

$$\bar{\boldsymbol{v}}_I = \begin{bmatrix} \bar{v}_{1I} \\ \bar{v}_{2I} \end{bmatrix}. \tag{4.28}$$

Let $\boldsymbol{e_n} = [\, e_{nx} \quad e_{ny} \,]$ and $\boldsymbol{e_s} = [\, e_{sx} \quad e_{sy} \,]$ be the unit vectors along the normal and tangential direction respectively, as shown in Fig. 23. The normal and tangential velocities can be expressed as

$$\bar{v}_n = [\, e_{nx} \quad e_{ny} \,] \begin{bmatrix} \bar{v}_1 \\ \bar{v}_2 \end{bmatrix} = \boldsymbol{R}_n \bar{\boldsymbol{v}} = \sum_I \boldsymbol{R}_n \boldsymbol{N}_I \bar{\boldsymbol{v}}_I, \tag{4.29}$$

where

$$\boldsymbol{R}_n = [\, e_{nx} \quad e_{ny} \,], \tag{4.30}$$

$$\bar{v}_s = [\, e_{sx} \quad e_{sy} \,] \begin{bmatrix} \bar{v}_1 \\ \bar{v}_2 \end{bmatrix} = \boldsymbol{R}_s \bar{\boldsymbol{v}} = \sum_I \boldsymbol{R}_s \boldsymbol{N}_I \bar{\boldsymbol{v}}_I, \tag{4.31}$$

$$\boldsymbol{R}_s = [\, e_{sx} \quad e_{sy} \,]. \tag{4.32}$$

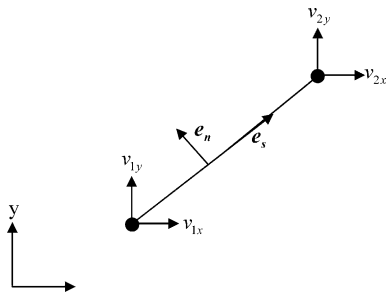

Fig. 23. Typical grain boundary element.

4.4. Grain boundary node distribution

During grain boundary migration the nodal density can vary significantly within the boundary segments of each grain as shown in Fig. 24. The situation is further amplified when topological changes occur. Thus it is needed to redistribute the finite element nodes along the grain boundary with arbitrary boundary shape.

The redistribution of nodes can be obtained by first fitting a smooth curve (Fig. 24) through the nodes using one-dimensional MLS/RK shape functions, and then redistribute the nodes along the parametric coordinate of the fitted curve. Following Chen and Wang [5], this is accomplished by first defining a nodal parametric coordinate as shown in Fig. 25. First, the parametric coordinates of the current particles on the grain boundary are defined by

$$\xi_I = \sum_{L=1}^{I-1} l_L \Big/ \sum_{L=1}^{M-1} l_L, \quad l_L = \|\boldsymbol{x}_{L+1} - \boldsymbol{x}_L\|. \tag{4.33}$$

Next, MLS/RK shape function $\{\Psi_I^c\}_{I=1}^M$ based on the nodal positions of the discrete points on the parametric coordinate are constructed as

$$\Psi_I^c(\xi) = \mathbf{H}^{\mathrm{T}}(0)\mathbf{M}^{-1}(\xi)\mathbf{H}(\xi - \xi_I)\Phi_a(\xi - \xi_I), \tag{4.34}$$

where $\boldsymbol{H}$ is the vector of basis functions

$$\boldsymbol{H}^{\mathrm{T}}(\xi - \xi_I) = [1, \xi - \xi_I] \tag{4.35}$$

Fig. 24. Nodal distribution on a discretized grain boundary during evolution.

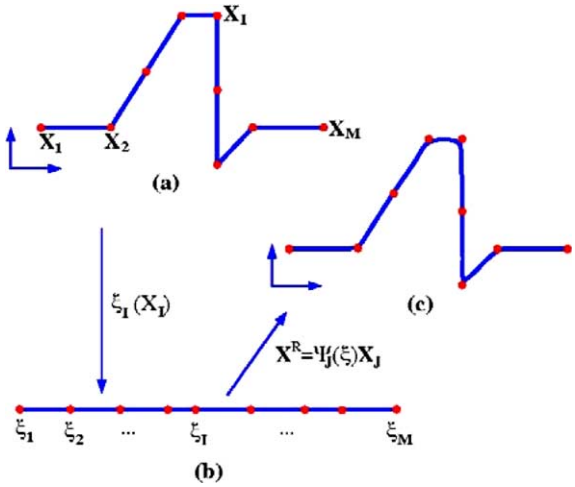

Fig. 25. Smooth curve approximation of a grain boundary with arbitrary shape: (a) master curve, (b) parametric domain and (c) RK approximation.

and the Gram Matrix $\boldsymbol{M}$ is

$$\boldsymbol{M}(\xi) = \sum_{I=1}^{M} \boldsymbol{H}(\xi - \xi_I)\boldsymbol{H}^{\mathrm{T}}(\xi - \xi_I)\Phi_a(\xi - \xi_I). \tag{4.36}$$

The RK shape functions are used to represent the grain boundary as

$$\boldsymbol{x}^R(\xi) = \sum_{I=1}^{M} \Psi_I^c(\xi)\boldsymbol{x}_I. \tag{4.37}$$

The new distribution of the nodes can be obtained by choosing equal incremental values of ξ in Eq. (4.37) as

$$\boldsymbol{x}_J^R = \boldsymbol{x}^R(\xi_J) = \sum_{I=1}^{M} \Psi_I^c(\xi_J)\boldsymbol{x}_I, \quad \xi_J = \frac{J}{M}, \quad J = 1, 2, \ldots, M. \tag{4.38}$$

In this work, the Kernel function Φ_a is a cubic spline function. Figs. 26 and 27 demonstrate the redistribution of nodes using the above method.

4.5. Discrete equations of stressed grain growth

By substituting approximations of $\boldsymbol{v}$ and $\bar{\boldsymbol{v}}$ into the variational equation in Eq. (3.14), and considerate the arbitrariness of $\delta\boldsymbol{v}$ and $\delta\bar{\boldsymbol{v}}$, the following discrete equations are obtained:

1. Grain boundary evolution equation:

$$\boldsymbol{C}^{\mathrm{gb}}\bar{\boldsymbol{v}} + \boldsymbol{f}^{\mathrm{gb}} + \boldsymbol{f}^{\mathrm{st}} = 0, \tag{4.39}$$

$$\boldsymbol{C}_{IJ}^{\mathrm{gb}} = \sum_{i=1}^{NGB} \int_{\Gamma_i^{\mathrm{gb}}} \frac{1}{\mu}\bar{\boldsymbol{N}}_I^{\mathrm{T}}\boldsymbol{R}_n^{\mathrm{T}}\boldsymbol{R}_n\bar{\boldsymbol{N}}_J \,\mathrm{d}s, \tag{4.40}$$

$$\boldsymbol{f}_I^{\mathrm{gb}} = \sum_{i=1}^{NGB} [\gamma\bar{\boldsymbol{N}}_I^{\mathrm{T}}\boldsymbol{R}_s^{\mathrm{T}}]_{s_i^1}^{s_i^2} + \sum_{i=1}^{NGB} \int_{\Gamma_i^{\mathrm{gb}}} \gamma\frac{\bar{\boldsymbol{N}}_I^{\mathrm{T}}\boldsymbol{R}_n^{\mathrm{T}}}{R} \,\mathrm{d}s, \tag{4.41}$$

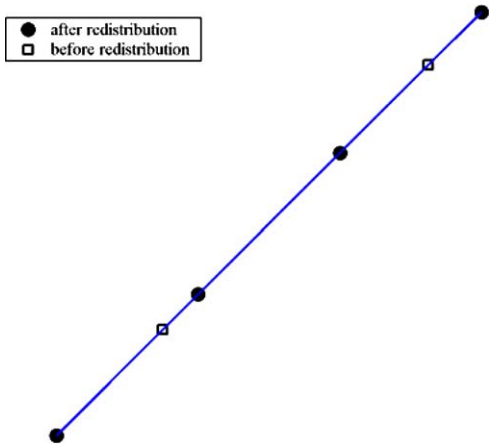

Fig. 26. Redistribution of the nodes on a straight grain boundary.

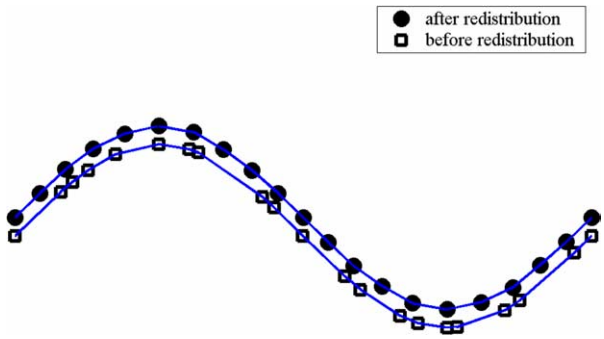

Fig. 27. Redistribution of nodes on a grain boundary with arbitrary shape.

$$\boldsymbol{f}_I^{\mathrm{st}} = \sum_{i=1}^{NGB} \int_{\Gamma_i^{\mathrm{gb}}} \frac{1}{2}(\boldsymbol{\sigma}^+ : \boldsymbol{\varepsilon}^+ - \boldsymbol{\sigma}^- : \boldsymbol{\varepsilon}^-)\boldsymbol{N}_I^{\mathrm{T}}\boldsymbol{R}_n^{\mathrm{T}}\,\mathrm{d}\Gamma, \tag{4.42}$$

where Γ_i^{gb} is the ith grain boundary segment, and NGB is the total number of grain boundary segment.

2. Grain deformation equation:

$$\boldsymbol{K}\boldsymbol{v} - (\boldsymbol{f}^{\mathrm{ext}} + \boldsymbol{f}^{\mathrm{bd}}) = \boldsymbol{0}, \tag{4.43}$$

$$\boldsymbol{K}_{IJ} = \int_{\Omega} \boldsymbol{B}_I^{\mathrm{T}}\boldsymbol{C}\boldsymbol{B}_J\,\mathrm{d}\Omega, \tag{4.44}$$

$$\boldsymbol{B} = \begin{bmatrix} \Psi_{I,1} & 0 \\ 0 & \Psi_{I,2} \\ \Psi_{I,2} & \Psi_{I,1} \end{bmatrix}, \tag{4.45}$$

$$\boldsymbol{C} = \begin{bmatrix} C_{1111} & C_{1122} & C_{1112} \\ C_{2211} & C_{2222} & C_{2212} \\ C_{1211} & C_{1222} & C_{1212} \end{bmatrix}, \tag{4.46}$$

$$\boldsymbol{f}_I^{\text{ext}} = \int_{\Gamma_h} \Psi_I \boldsymbol{h} \, \mathrm{d}\Gamma, \tag{4.47}$$

$$\boldsymbol{f}_I^{\text{bd}} = \int_{\Omega} \Psi_I \boldsymbol{b} \, \mathrm{d}\Omega. \tag{4.48}$$

Here, Eq. (4.39) governs the grain boundary velocity while Eq. (4.43) describes the material motion. At each time step, Eq. (4.39) is first solved and the grain boundary network under material deformation is updated. Eq. (4.43) is then solved based on the deformed grain network for the grain boundary migration velocity which again updates the grain network.

5. Numerical results

The following parameters are used in all numerical examples: *Box* size $= 1\ \mu\text{m} \times 1\ \mu\text{m}$, $\gamma_b = 0.5\ \mu\text{N}/\mu\text{m}$, $\mu = 0.1\ \mu\text{m}^3/\mu\text{N}\mu\text{s}$, $E_1 = 3 \times 10^5\ \mu\text{N}/\mu\text{m}^2$, $E_2 = 2 \times 10^5\ \mu\text{N}/\mu\text{m}^2$.

5.1. Uniform grain structure with a geometric imperfection

A stressed grain structure with a geometric imperfection in the middle is analyzed. A surface traction of uniform normal stress is applied in the horizontal direction. Two seven-side and two five-side grains were introduced at the center of a perfect hexagonal array as shown in Fig. 28(i). Each grain is considered isotropic.

This grain structure imperfection forces the grains to evolve primarily in response to the curvature-driven surface forces. The presence of the topological imperfections in the grain network triggers the time evolution of the microstructure; the driving force being the reduction of the free energy of the grain boundary network. As the time progresses the grain boundary migration via topology changes generates additional grains that are not six sided. In agreement with the von Newman relation [23,42], the grains with less than six edges continue to shrink and eventually disappear while those having more than six sides continue to grow. The time evolution of the microstructure is shown in Fig. 28(i)–(ix).

5.2. Uniform grain structure with a material inhomogeneity

In order to demonstrate the stress effect on the growth of an anisotropic grain structure, a network of uniform hexagonal grains is considered. Orthotropic material properties are introduced with the anisotropic orientation of one grain being different from the rest as shown in Fig. 29, and $E_1 > E_2$. The grain structure is subjected to a traction in the x-direction and periodic boundary conditions have been imposed. The following two cases are studied.

Case 1: The material orientations of the central (shaded) and surrounding grains are shown in Fig. 29. Under the applied external loading, the strain energy density in the central grain is higher than that of the surrounding grains and as a result this grain shrinks in order to reduce the total strain energy of the system. At the stage where the central grain shrinks to nearly a point, bifurcation occurs and topological changes result in one grain having more than seven edges and two grains having five edges. The grain with more than six edges continues to grow while the grains with less than six edges reduce in size and eventually disappear. The simulation results are shown in Fig. 29.

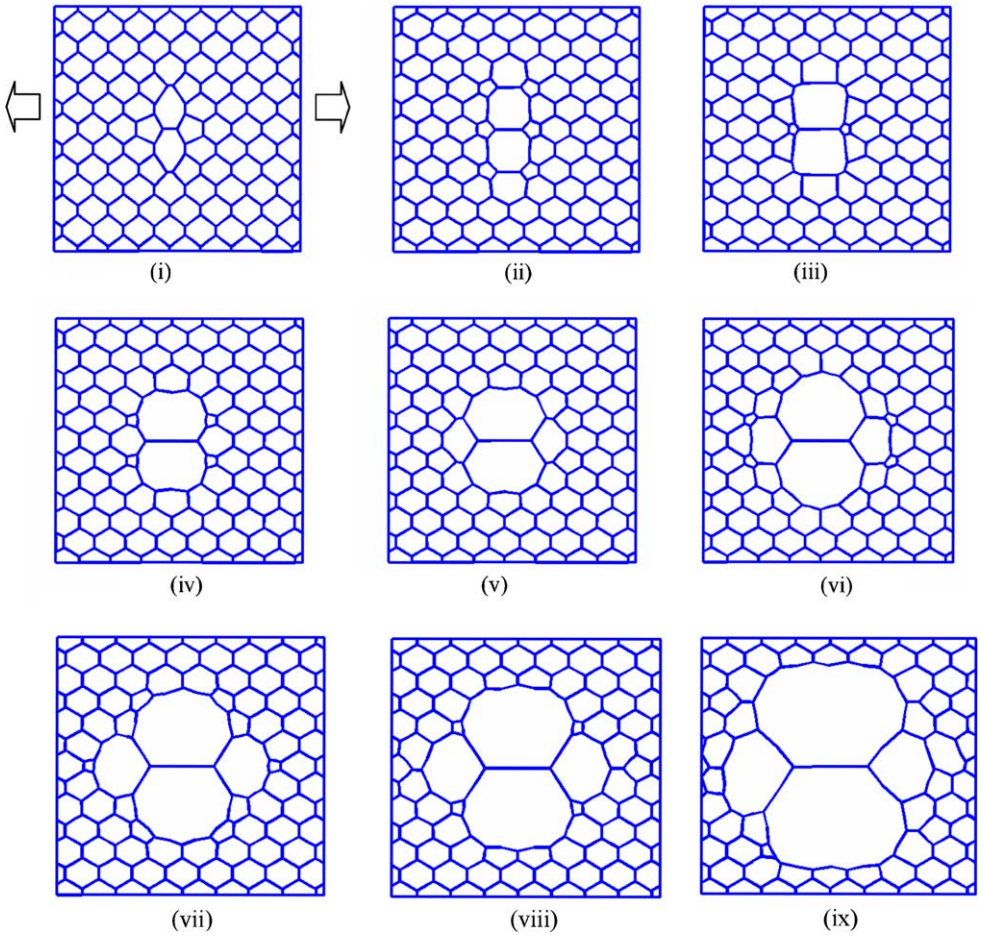

Fig. 28. Growth under stress of a balanced grain network with geometry imperfection.

Case 2: The material orientation are arranged to be opposite to the orientation considered in Case 1, as shown in Fig. 30. Under the applied external loading, the central grain (shaded) has a lower strain energy compared to the surrounding grains, and as a result, the central grain grows in size. Topological changes result in an unstable microstructure with the central grain having more than six edges while the grains surrounding the central grain have less than six edges. The simulation results are shown in Fig. 30.

5.3. Grain network with arbitrary grain structure

The random grain network shown in Fig. 31 is reanalyzed to study the grain growth of random grain structure and orientation angles under stress. The material anisotropic orientation angles are generated using a random number generator. Periodic boundary conditions have been imposed on the grain structure and the grain network is subjected to an applied traction from $h = 0$ to 9.4×10^6 $\mu N/\mu m^2$ in 0.188 s. Total of 470 steps, each with 0.0004 s is used. The periodic boundary conditions are imposed by kinematic constraints, and the enhanced MLS/RK shape functions that account for periodicity in the approximation are

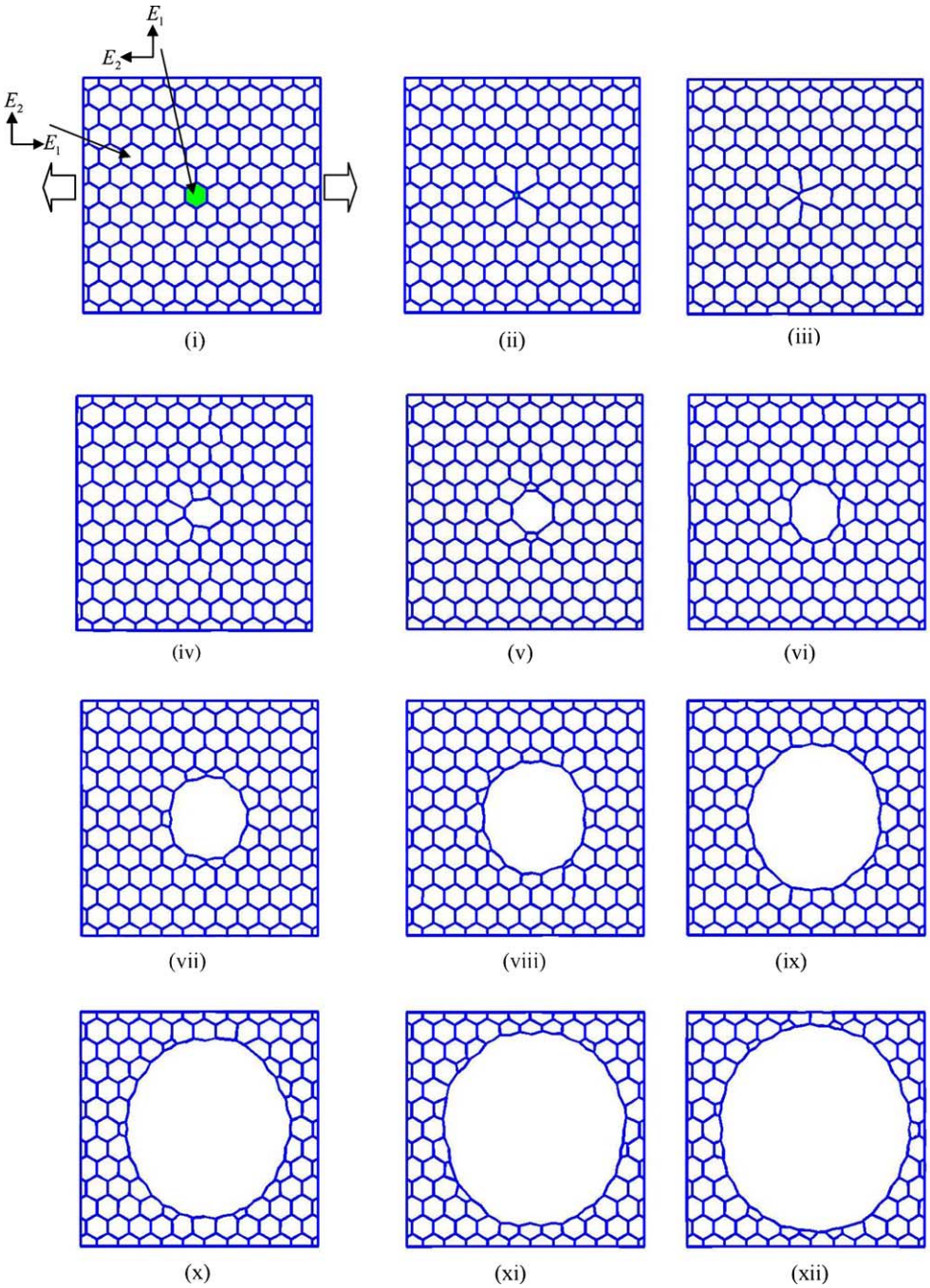

Fig. 29. Perfect grain structure with center grain assigned with larger strain energy density.

employed. The grain structure evolution processes shown in Fig. 31 are obtained with the proposed double-grid approach, and no remeshing is needed in the entire computation.

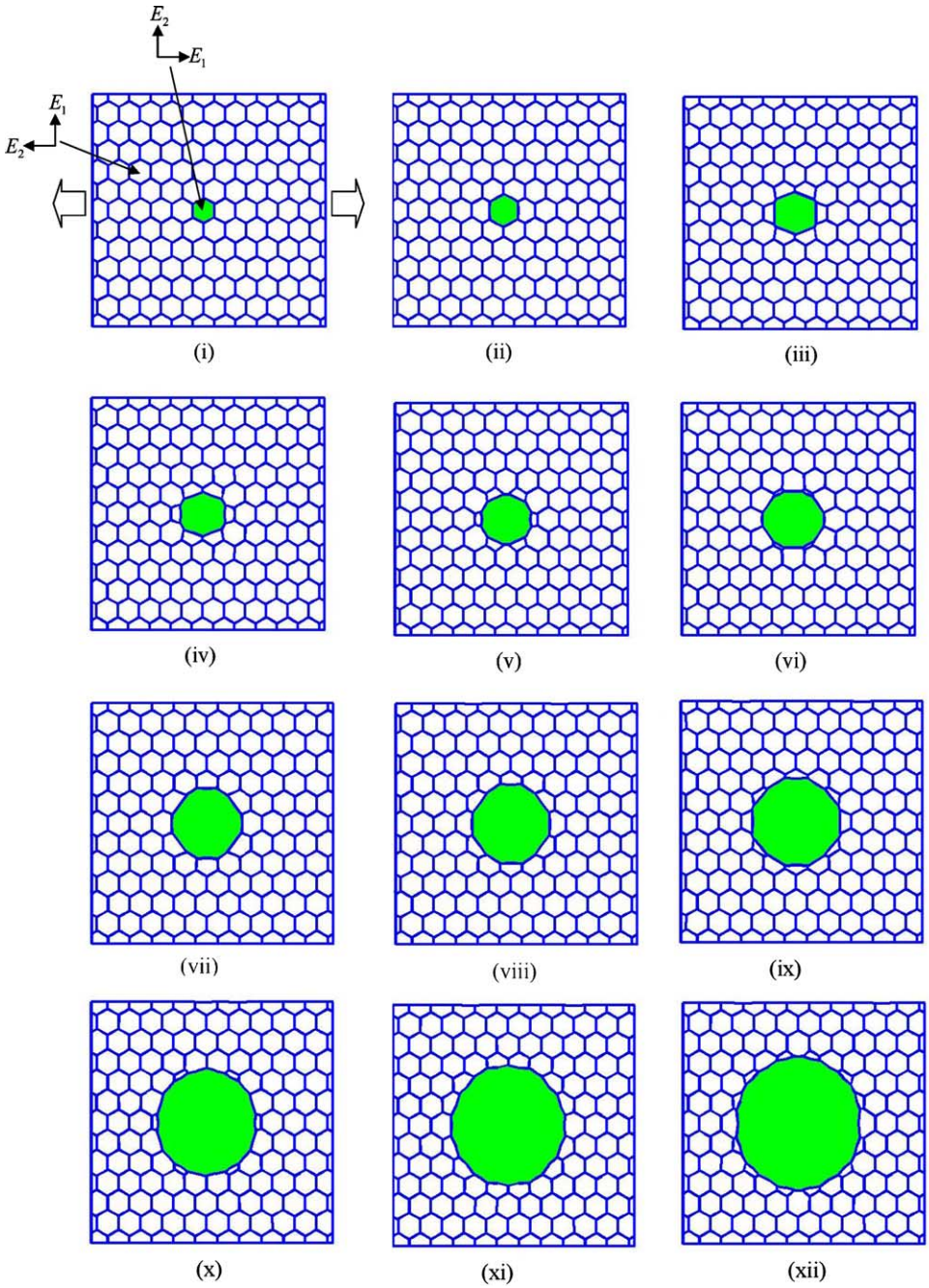

Fig. 30. Perfect grain structure with center grain assigned with lower strain energy density.

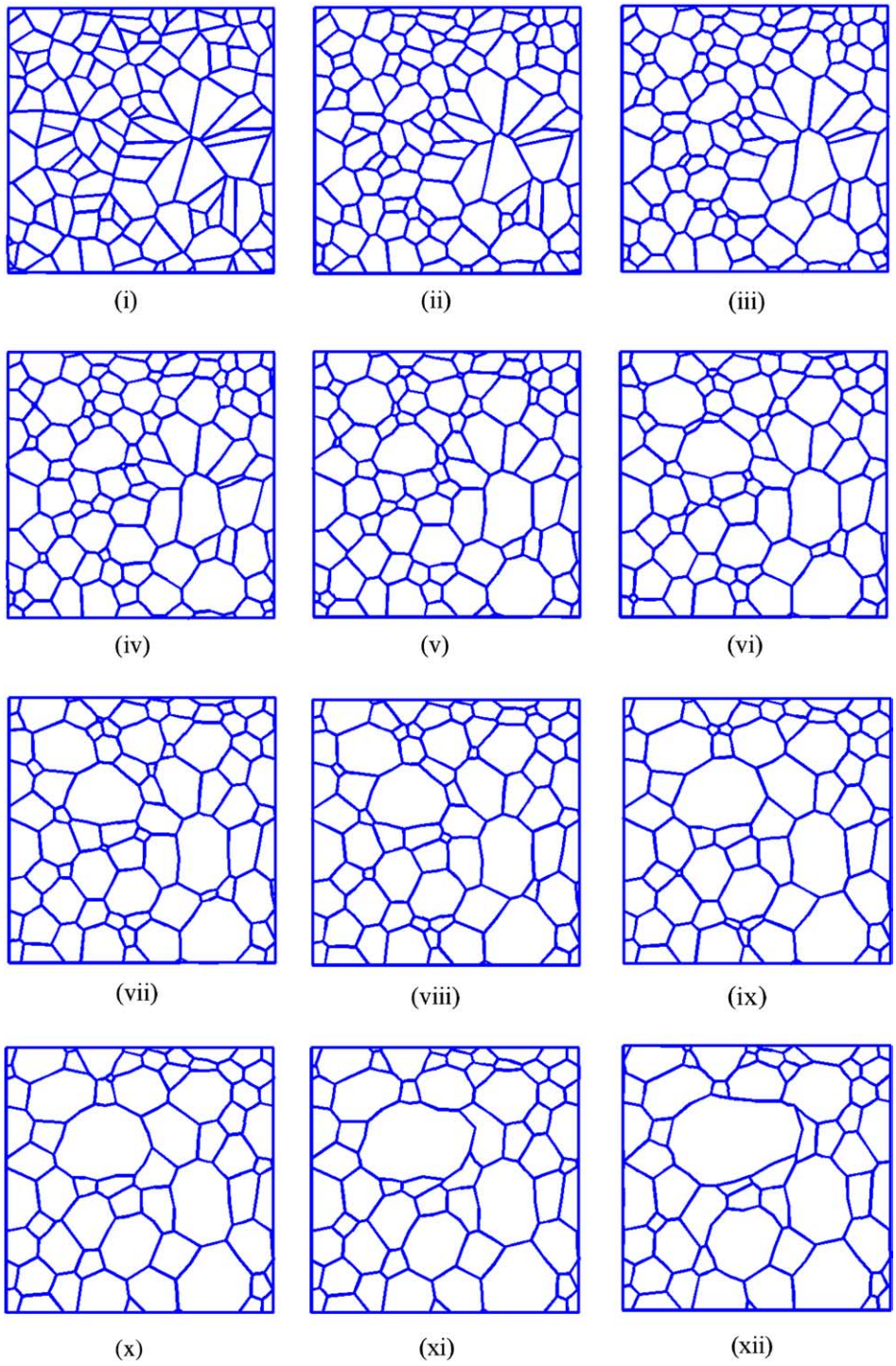

Fig. 31. Grain growth of an anisotropic arbitrary grain structure under stress.

6. Conclusions

A variational formulation and a double-grid discretization method for modeling stressed grain growth and grain boundary migration of polycrystalline materials have been introduced in this work. The variational equation was formulated based on the power balance of the system associated with grain boundary surface tension and curvature, grain boundary energy dissipation, rate of strain energy stored in each grain, strain energy density jump across the grain boundaries, and external work rate.

The numerical solution for stressed grain growth requires discretization of the grain boundaries as well as grain interiors. This presents a major difficulty in the discretization of the grain network with evolving topological changes. In this work, a double-grid method has been introduced. An interface-enriched moving least squares reproducing kernel (MLS/RK) approximation was used for the approximation of the material velocity, while the standard finite element method was used for the approximation of the grain boundary velocity. The coupling of the interface enrichment functions and the smooth MLS/RK shape functions was presented. It is also shown that the MLS/RK shape functions leads to significant errors near boundaries when imposing periodic boundary conditions. This is due to the nonlocality and truncation of MLS/RK near periodic boundaries. A modified MLS/RK approximation with implicit periodicity near boundaries has been introduced. This correction significantly enhances the solution of a periodic problem.

The proposed double-grid method completely eliminates the need for remeshing in modeling grain structure evolution. Several numerical examples have been tested to verify the effectiveness of the proposed method. These include perfect grain network problems with geometry and material imperfections and a random grain structure with random material orientation. The numerical results showed correct trend in the grain growth processes in these test problems.

References

[1] M.P. Anderson, D.J. Srolovitz, G.S. Grest, P.S. Sahni, Computer simulation of grain growth—I: kinetics, Acta Metall. 32 (1984) 783–791.
[2] H.V. Atkinson, Theories of normal grain growth in pure single phase systems, Acta Metall. 36 (1988) 469–491.
[3] T. Belytschko, Y.Y. Lu, L. Gu, Element-free Galerkin methods, Int. J. Numer. Methods Engrg. 37 (1994) 229–256.
[4] J.E. Burke, D. Turnbull, Recrystallization and grain growth, Progr. Metal Phys. 3 (1952) 220.
[5] J.S. Chen, H.P. Wang, Meshfree smooth surface contact algorithm for sheet metal forming, in: Proceeding of SAE 2000, Detroit, March 6–9, 2000.
[6] J.S. Chen, W. Han, Y. You, X. Meng, Reproducing kernel interpolation without finite element enrichment, Int. J. Numer. Methods Engrg. 56 (2003) 935–960.
[7] C.R. Chiang, The grain size effect on the flow stress of polycrystals, Scripta Metall. 19 (1985) 1281–1283.
[8] A.C.F. Cocks, S.P.A. Gill, A variational approach to two dimensional grain growth—I: theory, Acta Mater. 44 (1996) 4765–4775.
[9] A.C.F. Cocks, S.P.A. Gill, J. Pan, Modeling microstructure evolution in engineering materials, Adv. Appl. Mech. 36 (1999) 81–162.
[10] A.C.F. Cocks, The structure of constitutive laws for the sintering of fine grained materials, Acta Metall. Mater. 42 (1994) 2191–2210.
[11] L.W. Codes, B. Moran, Treatment of material discontinuity in the element-free Galerkin method, Comput. Methods Appl. Mech. Engrg. 139 (1996) 75–89.
[12] V.E. Fradkov, Two-dimensional normal grain growth: topological aspects, Adv. Phys. 43 (1994) 739–789.
[13] H.J. Frost, C.V. Thompson, C.L. Howe, J. Whang, A two-dimensional computer simulation of capillarity-driven grain growth: preliminary results, Scripta Metall. 22 (1988) 65–70.
[14] R.L. Fullman, Boundary migration during grain growth, Metal Interfaces, American Society for Metals, Cleveland, Ohio, 1952, pp. 179–207.
[15] Y. Han, M.C. Chaturvedi, J.R. Cahoon, Effect of grain size on the steady-state creep rate of inconel-718, Scripta Metall. 22 (1988) 255–260.
[16] A.J. Haslam, D. Moldovan, S.R. Phillpot, D. Wolf, H. Gleiter, Combined atomistic and mesoscale simulation of grain growth in nanocrystalline materials, Comput. Mater. Sci. 23 (2002) 15–32.

[17] A.J. Haslam, D. Moldovan, V. Yamakov, D. Wolf, S.R. Phillpot, H. Gleiter, Stress-enhanced grain growth in a nanocrystalline material by molecular-dynamics simulation, Acta Mater. 51 (2003) 2097–2112.
[18] K. Kawasaki, T. Nagai, K. Nakashima, Vertex models for two-dimensional grain growth, Philos. Mag. B 60 (1989) 399–421.
[19] Y. Krongauz, T. Belytschko, EFG approximation with discontinuous derivatives, Int. J. Numer. Methods Engrg. 146 (1996) 371–386.
[20] W.K. Liu, S. Jun, Y.F. Zhang, Reproducing kernel particle methods, Int. J. Numer. Methods Fluids 20 (1995) 1081–1106.
[21] W.K. Liu, S. Jun, S. Li, J. Adee, T. Belytschko, Reproducing kernel particle methods for structural dynamics, Int. J. Numer. Methods Engrg. 38 (1995) 1655–1679.
[22] R.M. McMeeking, L.T. Kuhn, A diffusional creep law for powder compacts, Acta Metall. Mater. 40 (1992) 961–969.
[23] D. Moldovan, D. Wolf, S.R. Phillpot, A.J. Haslam, Mesoscopic simulations of two-dimensional grain growth with anisotropic grain-boundary properties, Philos. Mag. A 82 (2002) 1271–1297.
[24] D. Moldovan, D. Wolf, S.R. Phillpot, A.J. Haslam, Role of grain rotation during grain growth in a columnar microstructure by mesoscale simulation, Acta Mater. 50 (2002) 3397–3414.
[25] J.E. Morral, M.F. Ashby, Dislocated cellular structures, Acta Metall. 22 (1974) 567–575.
[26] W.W. Mullins, Theory of thermal grooving, J. Appl. Phys. 28 (1957) 333.
[27] W.W. Mullins, Two dimensional motion of idealized grain boundaries, J. Appl. Phys. 27 (1956) 900.
[28] A. Needleman, J.R. Rice, Plastic creep flow effects in the diffusive cavitation of grain boundaries, Acta Metall. 28 (1980) 1315–1332.
[29] V.Yu. Novikov, Computer simulation of normal grain growth, Acta Metall. 26 (1978) 1739–1744.
[30] J. Pan, A.C.F. Cocks, A numerical analysis technique for the coupled surface and grain-boundary diffusion, Acta Metall. Mater. 43 (1995) 1395–1406.
[31] J. Pan, A.C.F. Cocks, Numerical simulation of superplastic deformation, Comput. Mater. Sci. 1 (1993) 95–109.
[32] P.S. Sahni, G.S. Grest, S.A. Safran, Kinetics of the Q-state potts model in two dimensions, Phys. Rev. Lett. 50 (1983) 263–266.
[33] B. Schönfelder, D. Wolf, S.R. Phillpot, M. Furtkamp, Molecular-dynamics method for the simulation of grain-boundary migration, Interf. Sci. 5 (1997) 245–262.
[34] C.S. Smith, Grain shapes and other metallurgical applications of topology, Metal Interfaces, American Society for Metals, Cleveland, Ohio, 1952, pp. 65–108.
[35] A. Soares, A.C. Ferro, M.A. Fortes, Computer simulation of grain growth in a bidimensional polycrystal, Scripta Metall. 19 (1985) 1491–1496.
[36] B. Sun, Z. Suo, A finite element method for simulating interface motion—II: Large shape change due to surface diffusion, Acta Mater. 45 (1997) 953–4962.
[37] Z. Suo, W. Wang, Diffusive void bifurcation in stressed solid, J. Appl. Phys. 76 (1994) 3410–3421.
[38] J. Svoboda, I. Turek, On diffusion-controlled evolution of closed solid-state thermodynamic systems at constant temperature and pressure, Philos. Mag. B 64 (1991) 749–759.
[39] C.V. Thompson, Grain growth and evolution of other cellular structures, Solid State Phys. 55 (2000) 269–314.
[40] D. Turnbull, Phase changes, Solid State Phys. 3 (1956) 225.
[41] M. Upmanyu, R.W. Smith, D.J. Srolvitz, Atomistic simulation of curvature driven grain boundary migration, Interf. Sci. 6 (1998) 41–58.
[42] J. von Neumann, Discussion remark concerning paper of C.S. Smith, Grain shapes and other metallurgical applications of topology, American Society for Metals, Cleveland, Ohio, 1952, pp. 108–110.
[43] D. Wang, J.S. Chen, L. Sun, Homogenization of magnetostrictive particle-filled elastomers using meshfree method with interface discontinuity, Finite Element Anal. Des. 39 (2003) 765–782.
[44] D. Weygand, Y. Brechet, A vertex dynamics simulation of grain growth in two dimensions, Philos. Mag. B 78 (1998) 329–352.